INTERNATIONAL JOURNAL OF CHEMICAL REACTOR ENGINEERING

Volume 1 2003 *Article* A44

Gas Dispersion and Bubble-to-Emulsion Phase Mass Exchange in a Gas-Solid Bubbling Fluidized Bed: A Computational and Experimental Study

Dhaneshwar J. Patil* Martin van Sint Annaland†

J.A.M. Kuipers‡

*University of Twente, dhaneshwar.patil@akzonobel-chemicals.com

†Twente University, M.vansintannaland@ct.utwente.nl

‡University of Twente, J.A.M.Kuipers@ct.utwente.nl

ISSN 1542-6580

Gas Dispersion and Bubble-to-Emulsion Phase Mass Exchange in a Gas-Solid Bubbling Fluidized Bed: A Computational and Experimental Study

Dhaneshwar J. Patil, Martin van Sint Annaland, and J.A.M. Kuipers

Abstract

Knowledge of gas dispersion and mass exchange between the bubble and the emulsion phases is essential for a correct prediction of the performance of fluidized beds, particularly when catalytic reactions take place. Test cases of single rising bubble and a bubbling fluidized bed operated with a jet without a chemical reaction were studied in order to obtain fundamental insights in the prevailing mass transfer phenomena. Numerical simulations were carried out to predict the dispersion of tracer gas using a two-fluid model based on Kinetic Theory of Granular Flow (KTGF). The simulations of a single-bubble rising through an incipiently fluidized bed revealed that the assumptions often made in phenomenological models in the derivation of correlations for the mass transfer coefficient, mainly that the bubble diameter remains constant and that the tracer concentration is uniform in the bubble, are not valid. The predicted bubble-to-emulsion phase mass transfer coefficient showed good agreement with the estimated values from the literature correlations assuming additive convection-diffusion transport for different bubble sizes and different particle sizes, indicating the importance of the convective distribution even for relatively small particles. Experiments were carried out to measure the steady state concentration profiles of a tracer gas in a pseudo two-dimensional bubbling fluidized bed operated with a jet. The simulated steady state concentration profiles of the tracer gas agreed well the experimental measurements. The radial convection of the gas is significantly influenced by the bubble 'throughflow' and therefore depends upon the particle and bubble size. The experimental comparison of theoretical results was extended to study the influence of the jet velocity and the particle diameter on the radial dispersion of the tracer gas in the bed.

KEYWORDS: CFD, Fluidization, KTGF, gas dispersion, bubbling fluidized bed

1. INTRODUCTION

In a gas-solid bubbling fluidized bed the gas passes in a complex manner through the bed as a result of the movement of the solids and the bubbling action. Detailed knowledge of gas dispersion and mass exchange between the bubble and the emulsion phases is essential for a correct prediction of the performance of fluidized beds, particularly when catalytic reactions take place. Most phenomenological models used to describe gas dispersion are variations of two-phase models, which consider a bubble phase and an emulsion phase. However, even the most sophisticated phenomenological model relies on experimentally determined correlations for the bubble size distribution and the mass transfer coefficient for the transport between the bubble and the emulsion phase (Werther, 1977; Krishna, 1981). Many of the correlations for the mass transfer coefficients are based on single-bubble measurements. The validity of these correlations for bubbling fluidized beds is, however, questionable. With the increasing computational power, numerical simulation has become a valuable tool to study fluid dynamics in multiphase flows. In recent years remarkable progress has been made in the modeling of the gas-solid flow in bubbling fluidized beds. Although some attempts have been made to predict the overall chemical conversion in fluidized beds with state of art hydrodynamic models (Guenther et al., 2001; Samuelsberg, 1994), a detailed study on the gas dispersion and mass exchange between the bubble and the emulsion phase without chemical reactions is an important first step for a correct interpretation of all the phenomena occurring in a fluidized bed, which is the objective of this work.

Numerical simulations were carried out to predict the dispersion of tracer gas using a two-fluid model based on conservation equations for total mass, momentum and species. The internal momentum transfer in the particulate phase was described with the Kinetic Theory of Granular Flow (KTGF). Simulations for a single rising bubble and a bubbling fluidized bed were performed in order to obtain fundamental insights in the prevailing mass transfer phenomena. The model predictions for the steady state concentration profiles of the tracer gas, which was introduced into the bed through a jet, were compared with experimental results obtained in a pseudo two-dimensional bed operated with different jet velocities.

In this article, firstly, the experimental setup with which the steady state concentration of tracer gas was measured in bubbling fluidized bed operated with a jet is shortly discussed. Subsequently, the two-fluid model and the closure equations are described. The simulation results for the transport of tracer gas from a single rising bubble through an incipiently fluidized bed are described in order to validate the assumptions often made in the literature in the derivation of correlations for the bubble-to-emulsion phase mass transfer coefficients. The bubble-to-emulsion phase mass transfer coefficient is calculated from the simulation results and compared with correlations taken from the literature to determine the dominant mechanism for bubble-to-emulsion phase mass transfer for different bubble and particle sizes. Then, for a bubbling fluidized bed with a continuous jet in center, the radial dispersion of tracer gas introduced in the bed via the jet is investigated and compared with the experimental results. The influence of jet velocity as well as particle size on the radial dispersion of the tracer gas is studied.

2. EXPERIMENTS

The main objective of the experimental program was to measure the steady state concentration of a CO_2 tracer gas introduced in a pseudo two-dimensional (0.3 m × 1.0 m × 0.015 m) gas-solid fluidized bed via a jet in the center of the bed. The tracer gas was mixed with fluidizing gas before injecting it with a velocity well above the minimum fluidization velocity into a bed filled to a height of 0.4 m with glass beads of 460 μm diameter. To ensure that the tracer was well mixed with fluidizing gas, a wire mesh was inserted just above the introduction point of the tracer gas (see Figure 1). Uniform background fluidization (just above incipient fluidization) was achieved via a porous plate distributor and additionally inlet section was filled with glass beads (100 μm). Physical properties of the fluidizing gas and the particles have been listed in Table 1.

The concentrations of CO_2 were measured with an IR (infra red) analyzer where gas was extracted from the bed via a probe. The probe consisted of a 2 mm tube with a gauze at the end of the tube to avoid blockage by particles. The probe could be transversed to measure the tracer concentration at different locations. A pump was used to maintain a small steady flow of sample gas to the CO_2 analyzer.

A computer program was developed for the automatic acquisition of the measured concentrations. The steady state concentration was obtained by averaging over 100 data points. With this measurement procedure good reproducibility was assured.

Table 1: Physical properties of the particles and fluidizing gas.

Particle diameter [μm]	460	700
Particle density [kg/m^3]	2660	2660
Restitution coefficient	0.95	0.95
Gas density [kg/m^3]	1.2	1.2
Gas viscosity [Pa·s]	1.85×10^{-5}	1.85×10^{-5}
Diffusivity of CO_2 [m^2/s]	2.00×10^{-5}	2.00×10^{-5}
u_{mf} [m/s]	0.19	0.42

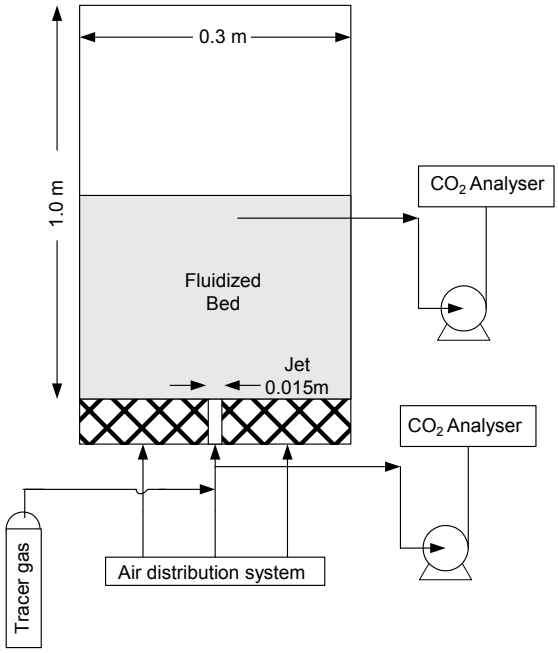

Figure 1: Schematic representation of the experimental setup.

3. MODEL DESCRIPTION

For the description of the hydrodynamic behavior of fluidized beds, Two-Fluid (Eulerian-Eulerian) models have been developed, which are based on the conservation equations for mass and momentum for both the gas and solid phases supplemented with a species conservation equation (see Table 2). Newtonian behavior was assumed for the gas phase stress tensor.

$$\boldsymbol{\tau}_f = -\left[\left(\lambda_f - \frac{2}{3}\mu_f\right)\left(\nabla\cdot\overline{\boldsymbol{u}}\right)\boldsymbol{I} + \mu_f\left((\nabla\overline{\boldsymbol{u}}) + (\nabla\overline{\boldsymbol{u}})^T\right)\right] \tag{1}$$

Here, μ_g is the gas phase viscosity, λ_g is the gas phase bulk viscosity which is assumed zero and $\boldsymbol{I}$ is the unit tensor.

Table 2: Conservation equations

Continuity equation:

Gas phase:

$$\frac{\partial(\varepsilon_f \rho_f)}{\partial t} + \nabla \cdot (\varepsilon_f \rho_f \bar{\boldsymbol{u}}) = 0 \tag{2}$$

Solid phase:

$$\frac{\partial(\varepsilon_s \rho_s)}{\partial t} + \nabla \cdot (\varepsilon_s \rho_s \bar{\boldsymbol{v}}) = 0 \tag{3}$$

Momentum equation:

Gas phase:

$$\frac{\partial(\varepsilon_f \rho_f \bar{\boldsymbol{u}})}{\partial t} + \nabla \cdot (\varepsilon_f \rho_f \bar{\boldsymbol{u}}\,\bar{\boldsymbol{u}}) = -\varepsilon_f \nabla p - \beta(\bar{\boldsymbol{u}} - \bar{\boldsymbol{v}}) - (\nabla \cdot \varepsilon_f \boldsymbol{\tau}_f) + \varepsilon_f \rho_f \boldsymbol{g} \tag{4}$$

Solid phase:

$$\frac{\partial(\varepsilon_s \rho_s \bar{\boldsymbol{v}})}{\partial t} + \nabla \cdot (\varepsilon_s \rho_s \bar{\boldsymbol{v}}\,\bar{\boldsymbol{v}}) = -\varepsilon_s \nabla p + \beta(\bar{\boldsymbol{u}} - \bar{\boldsymbol{v}}) - (\nabla \cdot \varepsilon_s \boldsymbol{\tau}_s) - \nabla p_s + \varepsilon_s \rho_s \boldsymbol{g} \tag{5}$$

Species conservation equation:

$$\frac{\partial(\varepsilon_f \rho_f \omega_{Af})}{\partial t} + \nabla \cdot \left(\varepsilon_f \left(\rho_f \bar{\boldsymbol{u}} \omega_{Af} - D_{eff,A} \nabla \omega_{Af} \right) \right) = 0 \tag{6}$$

The interphase momentum transfer is an important term in the modeling of gas-particle interactions since particle fluidization results from the drag exerted by the interstitial gas on the particulate phase. The form and the skin drag are combined in a single empirical parameter, the interphase momentum transfer coefficient, β. In the dense regime ($\varepsilon_f < 0.80$) the inter-phase momentum transfer coefficient was described with from the well-known Ergun equation (Ergun, 1952), which is based on the pressure drop measurement of packed beds.

$$\beta = 150 \frac{\left(1-\varepsilon_f\right)^2}{\varepsilon_f} \frac{\mu_f}{(\phi_s d_p)^2} + 1.75\left(1-\varepsilon_f\right) \frac{\rho_f}{\phi_s d_p} \left|\bar{\boldsymbol{u}} - \bar{\boldsymbol{v}}\right| \tag{7}$$

In more dilute regimes ($\varepsilon_f > 0.80$), the inter-phase momentum transfer coefficient has been derived from the correlation of Wen and Yu (1966). Wen and Yu (1966) have performed settling experiments of solid particles in a liquid over a wide range of solid volume fractions and have correlated their data and that of others for $0.01 \le \varepsilon_s \le 0.63$.

$$\beta = \frac{3}{4} C_d (1-\varepsilon_f) \frac{\rho_f}{\phi_s d_p} \left|\bar{\boldsymbol{u}} - \bar{\boldsymbol{v}}\right| \varepsilon_f^{-1.65} \tag{8}$$

where,

$$C_d = \frac{24}{\mathrm{Re}_p}(1 + 0.15(\mathrm{Re}_p)^{0.687}) \qquad \mathrm{Re}_p < 1000$$

$$C_d = 0.44 \qquad \mathrm{Re}_p > 1000 \tag{9}$$

$$\text{and } \mathrm{Re}_p = \frac{\varepsilon \rho_f \left|\bar{\boldsymbol{u}} - \bar{\boldsymbol{v}}\right| d_p}{\mu_f}$$

Since the interphase momentum transfer coefficient shows a discontinuity at ε_f=0.8, simulations were also carried out using more recent correlations e.g. as proposed by Koch and Hill (2001), which is based on detailed Lattice Boltzmann simulations. However, the results were not influenced by the correlation used.

3.1 Solid phase rheology

The two-fluid model requires constitutive equations to describe the internal momentum transfer in the solid phase, i.e. the solid phase pressure and shear stress tensor. Following the approach introduced by Savage (1983), it is assumed that the particulate stress tensor is the sum of the kinetic stress tensor and the frictional stress tensor (caused by long term or multi-particle contact and deformations), each contribution evaluated as if it acted separately. Although the physical basis for this assumption remains unproven, it captures the two extreme limits of granular flow: the rapid shear flow regime, where the kinetic and collisional contribution dominates and the quasi-static flow regime, where friction dominates. Thus, the solid phase pressure and solid phase viscosity are expressed as,

$$p_s = p_s^{kc} + p_s^f \tag{10}$$

and

$$\mu_s = \mu_s^{kc} + \mu_s^f \tag{11}$$

Here, the superscript *k* refers to the kinetic and collisional contribution and *f* refers to the frictional contribution.

3.1.1 Kinetic and collisional stress model

The kinetic and collsional contribution is modeled with the Kinetic Theory of Granular Flow (KTGF). As a result of shearing of the particulate phase in a fluidized bed, particles collide resulting in a random granular motion. This particle velocity fluctuation generates an effective pressure in the particulate phase, together with an effective viscosity that resists shearing of the particle assembly. Associated with the random motion of the particles, a granular temperature Θ_s can be defined as $\frac{3}{2}\Theta_s = \frac{1}{2}\overline{\boldsymbol{C}_s \cdot \boldsymbol{C}_s}$ where $\boldsymbol{C}_s$ is the random fluctuating velocity of the particulate phase. Modeling of the collisional and kinetic transport mechanisms for the momentum ($m\boldsymbol{C}_s$) and fluctuating kinetic energy of the particles ($1/2m\,\boldsymbol{C}_s^2$) (see e.g. Nieuwland, 1995) yields a description of the momentum transport properties as a function of the granular temperature, for which an additional transport equation is given by.

$$\frac{3}{2}\left\{\frac{\partial}{\partial t}(\varepsilon_s \rho_s \Theta_s) + \nabla\cdot(\varepsilon_s \rho_s \Theta_s \overline{\boldsymbol{v}})\right\} = -\left(P_s^{kc}\boldsymbol{I} + \varepsilon_s \boldsymbol{\tau}_s^{kc}\right) : \nabla \overline{\boldsymbol{v}} + \nabla\cdot\overline{q}_s - \gamma - \beta\left(\Theta_s - \left\langle\overline{\boldsymbol{C}_f \cdot \boldsymbol{C}_s}\right\rangle\right) \tag{12}$$

The two terms on the left hand side of equation (12) represent the accumulation and convection of kinetic fluctuation energy. On the right hand side of equation (12), the first term describes the production of kinetic fluctuation energy due to irreversible deformation of the velocity fields. The second term models the conductive transport of kinetic fluctuation energy. The third term represents the fluctuation energy dissipation due to inelastic particle-particle interactions. The fourth term represents the exchange of the fluctuation energy due to interphase momentum transport. The $\left\langle\overline{\boldsymbol{C}_f \cdot \boldsymbol{C}_s}\right\rangle$ term representing the interaction between the fluctuating gas velocity and the fluctuating particle velocity is neglected because gas phase turbulence is completely suppressed in bubbling gas-solid fluidized beds. For the derivation of this conservation equation and the subsequent constitutive equations the interested reader is referred to the books by Chapman and Cowling (1970) and Gidaspow (1994) and the papers by Jenkins and Savage (1983), Ding and Gidaspow (1990) and Nieuwland et al. (1996). The constitutive equations are listed in Table 3.

3.1.2 Frictional stress model

At high solids volume fractions, individual particles interact with multiple neighbors with sustained contact, where normal reaction forces and associated tangential frictional forces at these sliding contacts are dominant. The friction model presented by Atkinson and Brandsbey (1978) and Jackson (1982) based on the critical state theory of soil mechanics was used in this work. In a recent model, Srivastava and Sundaresan (2003) took into account the

argument put forward by Savage (1998) that even in a purely quasi-static flow fluctuations exists in the strain rate associated with the formation of a shear layer and these fluctuations will decrease the shear stress in the particle assembly. The authors suggested an ad hoc modification, which recognizes the effect of strain rate fluctuations in an approximate manner. The frictional stresses were described as,

$$p_s^f = p_c\left(\varepsilon_s\right) \tag{13}$$

$$\mu_s^f = \frac{p_c\left(\varepsilon_s\right)\sqrt{2}\sin\phi}{2\varepsilon_s\sqrt{\left(\overline{\overline{D}}_{ij} : \overline{\overline{D}}_{ij} + \Theta_s/d_p^2\right)}} \tag{14}$$

$$\overline{\overline{D}}_{ij} : \overline{\overline{D}}_{ij} = \left(\frac{1}{2}\left(\left(\nabla\overline{\boldsymbol{v}}\right)+\left(\nabla\overline{\boldsymbol{v}}\right)^T\right)-\left(\frac{1}{3}\nabla\cdot\overline{\boldsymbol{v}}\right)\boldsymbol{I}\right)$$

where, ϕ is the angle of internal friction and $p_c\left(\varepsilon_s\right)$ is the critical state pressure, which can be expressed as (Jonhanson and Jackson, 1987)

$$p_c\left(\varepsilon_s\right) = \begin{cases} F\dfrac{\left(\varepsilon_s-\varepsilon_{s,\min}\right)^r}{\left(\varepsilon_{s,\max}-\varepsilon_s\right)^s} & \varepsilon_s > \varepsilon_{s,\min} \\ 0 & \varepsilon_s < \varepsilon_{s,\min} \end{cases} \tag{15}$$

where *F, r* and *s* are empirical constants. Different values of *F*, *r*, and *s* were reported in the literature for different types and sizes of the particles. In this work *F, r* and *s* were assumed to be equal to 0.5, 2.0 and 3.0 respectively (Ocone *et al.*, 1993).

Table 3: Constitutive equations based on the kinetic theory of granular flow.

Solid phase pressure $p_s^{kc} = \varepsilon_s\rho_s\Theta_s + 2\left(1+e\right)\varepsilon_s^2 g_0\rho_s\Theta_s$	*Radial distribution function (Ma and Ahmadi, 1986)* $g_o = \dfrac{1+2.5\varepsilon_s+4.5904\varepsilon_s^2+4.515439\varepsilon_s^3}{\left[1-\left(\dfrac{\varepsilon_s}{\varepsilon_s^{\max}}\right)^3\right]^{0.67802}}$
Solids phase stress-tensor $\boldsymbol{\tau}_s^{kc} = -\left[\left(\lambda_s-\frac{2}{3}\mu_s^{kc}\right)\left(\nabla\cdot\overline{\boldsymbol{v}}\right)\overline{\overline{I}}+\mu_s\left(\left(\nabla\overline{\boldsymbol{v}}\right)+\left(\nabla\overline{\boldsymbol{v}}\right)^T\right)\right]$	
Solid phase shear viscosity $\mu_s^{kc} = \frac{4}{5}\rho_s d_p g_0\left(1+e\right)\left(\frac{\Theta_s}{\pi}\right)^{1/2} +$ $1.01600\frac{5}{16}\frac{m}{d_p^2}\left(\frac{\Theta_s}{\pi}\right)^{1/2}\frac{\left(1+\frac{4}{5}\left(1+e\right)\varepsilon_s g_0\right)\left(1+\frac{8}{5}\varepsilon_s g_0\right)}{\varepsilon_s g_0}$	*Conductivity of particulate fluctuating energy* $\kappa_s = 2\varepsilon_s\rho_s d_p g_0\left(1+e\right)\left(\frac{\Theta_s}{\pi}\right)^{1/2} +$ $1.02513\frac{75}{64}\frac{m}{d_p^2}\rho_s d_p\left(\frac{\Theta_s}{\pi}\right)^{1/2}\frac{\left(1+\frac{6}{5}\left(1+e\right)\varepsilon_s g_0\right)\left(1+\frac{12}{5}\varepsilon_s g_0\right)}{\varepsilon_s g_0}$
Solid phase bulk viscosity $\lambda_s = \frac{4}{3}\rho_s d_p g_0\left(1+e\right)\left(\frac{\Theta_s}{\pi}\right)^{1/2}$	*Dissipation due to inelastic collisions* $\gamma = 3\left(1-e^2\right)\varepsilon_s^2\rho_s g_0\Theta_p\left(\frac{4}{d_p}\left(\frac{\Theta_s}{\pi}\right)^{1/2}-\nabla\cdot\overline{\boldsymbol{v}}\right)$

3.2 Effective gas diffusivity in a fluidized bed reactor

Transport of the tracer gas in a fluidized bed takes place due to convection and molecular diffusion. Micro scale convection transport takes place on the subgrid scale can be accounted for in the Eulerian modeling framework via an effective diffusivity, which is a function of the local porosity and gas phase velocity. Thus, the total effective diffusivity consists of a contribution due to molecular diffusion and a contribution due to micro-scale convective patterns, analogous to the description of mass dispersion in packed bed reactors.

The contribution due to molecular diffusion corrected for the tortuous path in a packed bed induced by the presence of the solids following Punčochář and Drahoš (1993), and the contribution of the subgrid scale convection to the effective diffusivity taken from Gunn (1987) for a packed bed, and slightly adopted for a fluidized bed, is modeled as,

$$\varepsilon_f D_{eff} = \varepsilon_f \sqrt{\varepsilon_f} D_{mol} + \frac{\varepsilon_s}{\varepsilon_{s.\max}} \frac{\varepsilon_f \left| \bar{\boldsymbol{u}} - \bar{\boldsymbol{v}} \right| d_p}{40 - 29 \exp(-7 / \mathrm{Re}_p)} \tag{16}$$

with,

$$\mathrm{Re}_p = \frac{\varepsilon \rho_f \left| \bar{\boldsymbol{u}} - \bar{\boldsymbol{v}} \right| d_p}{\mu_f}$$

3.3 Boundary conditions

The gas velocities were assumed to obey the no-slip condition, while the solids were allowed to slip along the wall, following the boundary conditions given by Sinclair and Jackson (1989) based on a microscopic model for particle-wall collisions:

$$\begin{aligned} (\boldsymbol{I} - \bar{\boldsymbol{n}}\bar{\boldsymbol{n}}) \cdot \varepsilon_s \boldsymbol{\tau}_s \cdot \bar{\boldsymbol{n}} &= \frac{\alpha_s \pi \varepsilon_s \rho_s g_0 \sqrt{\Theta_s}}{2\sqrt{3}\varepsilon_s^{\max}} \boldsymbol{v} \\ \varepsilon_s \bar{q}_s \cdot \bar{\boldsymbol{n}} &= -\boldsymbol{v} \cdot \varepsilon_s \boldsymbol{\tau}_s \cdot \bar{\boldsymbol{n}} + \frac{\sqrt{3}\pi \left(1 - e_w^2\right) \varepsilon_s \rho_s g_0 \Theta_s^{\frac{3}{2}}}{4\varepsilon_s^{\max}} \end{aligned} \tag{17}$$

In our study the values for the coefficient of restitution for particle-wall collisions e_w and the specularity coefficient α_s were taken as 0.9 and 0.5, respectively. Dankwert's boundary conditions were used for the inlet and outlet for the species mass conservation equation while the walls were assumed impermeable.

4. NUMERICAL SIMULATIONS

The two-fluid model equations were implemented in the commercial CFD code CFX4.4 from AEA Technology, Harwell, UK. For evaluation of the convective terms the third order total variation diminishing (TVD) scheme min-mod was used. Single bubble simulations were carried out for a two-dimensional fluidized bed of size 0.57 m × 0.75 m equipped with a jet (width 0.015 m) in the center of the bed, for particles of 460 and 100 μm (taking the same properties for particles as listed in Table 1). Also continuous jet simulations were carried out to predict the steady state concentration profiles of the tracer gas inside a two-dimensional fluidized bed of size 0.3 m × 1.0 m for two different particle sizes (460 μm and 700 μm) (see Table 1). Grid dependency of the simulated results was checked using different grid sizes (0.01 m × 0.0075 m; 0.005 m × 0.005 m and 0.0025 m × 0.0025 m). Calculations have shown that with a uniform grid of 0.005 m in the vertical and the horizontal direction a grid independent solution was obtained, where a time step of 1×10^{-4} s was used.

5. SINGLE BUBBLE SIMULATIONS

5.1 Classical approach

Over the years, a number of phenomenological models have been proposed for the prediction of gas dispersion in a fluidized bed. These models are variations of two-phase models containing parameters, which must be determined experimentally. These parameters include the bubble diameter and the bubble-to-emulsion phase mass transfer coefficient. In the most advanced phenomenological models, the bubble size variation along the bed height is included via experimental correlations. However, for the mass transfer coefficient between the bubble and the emulsion phase a correlation was used based on single-bubble measurements in which a single isolated bubble of tracer gas is introduced in a fluidized bed at incipiently fluidization conditions and initially free from tracer gas. In these correlations the effect of the presence of other bubbles on the mass transfer coefficient was not taken into account. The mass transfer coefficient was correlated from the experiments, where the concentration of a tracer gas in the bubble was measured at different heights in the fluidized bed, making use of the following assumptions

1. The bubble diameter is constant while rising through the bed.
2. The concentration of a tracer gas is uniform inside the bubble.
3. The mass transfer coefficient remains constant.

However, validity of these assumptions is unclear and it is the purpose of this work to clarify their validity using detailed numerical models.

In the literature, there are many correlations available for the prediction of the bubble-to-emulsion phase mass transfer coefficient. However, the correlations are based on assumptions on the dominating transport mechanism (diffusion controlled versus convection-diffusion controlled etc.) and their predictions differ even in the order of magnitude. Examples of different approaches to estimate the mass transfer coefficient have been listed in Table 4. In the diffusion-controlled models, the interphase mass transfer rate is assumed to be limited by diffusion across the cloud boundary, obviously implicitly assuming that cloud formation occurs. In the additive convection-diffusion approach, the controlling resistance to mass transfer is assumed to reside at the bubble interface and the mass transfer is assumed to occur by convection (bubble throughflow) and diffusion, where the individual contributions were evaluated separately and subsequently summed.

Table 4: Different phenomenological models from the literature representing the typical class of the model.

Approach	Mass transfer coefficient (m/s)
Diffusion Controlled Chiba and Kobayashi (1970)	$k_m = k_{bc} = \sqrt{\frac{4 D_f \varepsilon_{mf}^2 u_b (\alpha - 1)}{\pi D_c \alpha}}$
Additive convection-diffusion controlled Davidson and Harrison (1963) (assuming circular bubble)	$k_m = 0.6 D_f^{1/2} \left(g / D_b \right)^{1/4} + \frac{2 u_{mf}}{\pi}$

5.2 Results and discussion

5.2.1 Validity of the assumptions used in the phenomenological models

In this numerical study, the validity of the assumptions used in the in phenomenological model verified using detail simulations for a single bubble injected into a fluidized bed. The mass transfer coefficients predicted by the model are compared with the literature correlations, and the influence of the bubble diameter and the particle diameter on the mass transfer rate is studied.

In the simulations, a bubble was introduced into a bed maintained at minimum fluidization conditions via a jet with a gas velocity much higher than the minimum fluidization velocity. After the formation of the bubble (0.2 s), the jet velocity (7 m/s) was reduced to the minimum fluidization velocity, and equal to the gas velocity through the porous plate. The tracer gas was introduced through the jet only during the period of bubble formation. The bubble exchanges gas with the emulsion phase while rising through the bed. Snapshots of the volume fraction of the

gas phase and the mass fraction of tracer gas at different times in a fluidized bed filled with 460 μm particle are presented in Figure 2. The figure clearly shows that during the initial period of 0.2 s, a bubble was formed at the nozzle of the fluidized bed and the tracer gas is introduced in the bubble. Subsequently the bubble detaches from the nozzle and rises carrying the tracer gas with it, where the concentration of the tracer gas inside the bubble decreases due to dilution with emulsion gas at the bottom of the bubble while at the time tracer gas percolates into the emulsion phase at the top of the bubble. In addition the bubble shape changes from circular at 0.2 s to spherical cap at the top of the bed.

To enable a quantitative comparison of the model results with the predictions by phenomenological models it is necessary to define a bubble interface. A bubble interface was estimated from the calculated porosity distribution. A bubble diameter was defined as the diameter of a circle having the same area as the numerically computed area for which $\varepsilon_f > 0.85$. When the bubble boundary crosses a Eulerian grid cell, an interpolation technique was used to calculate the bubble area.

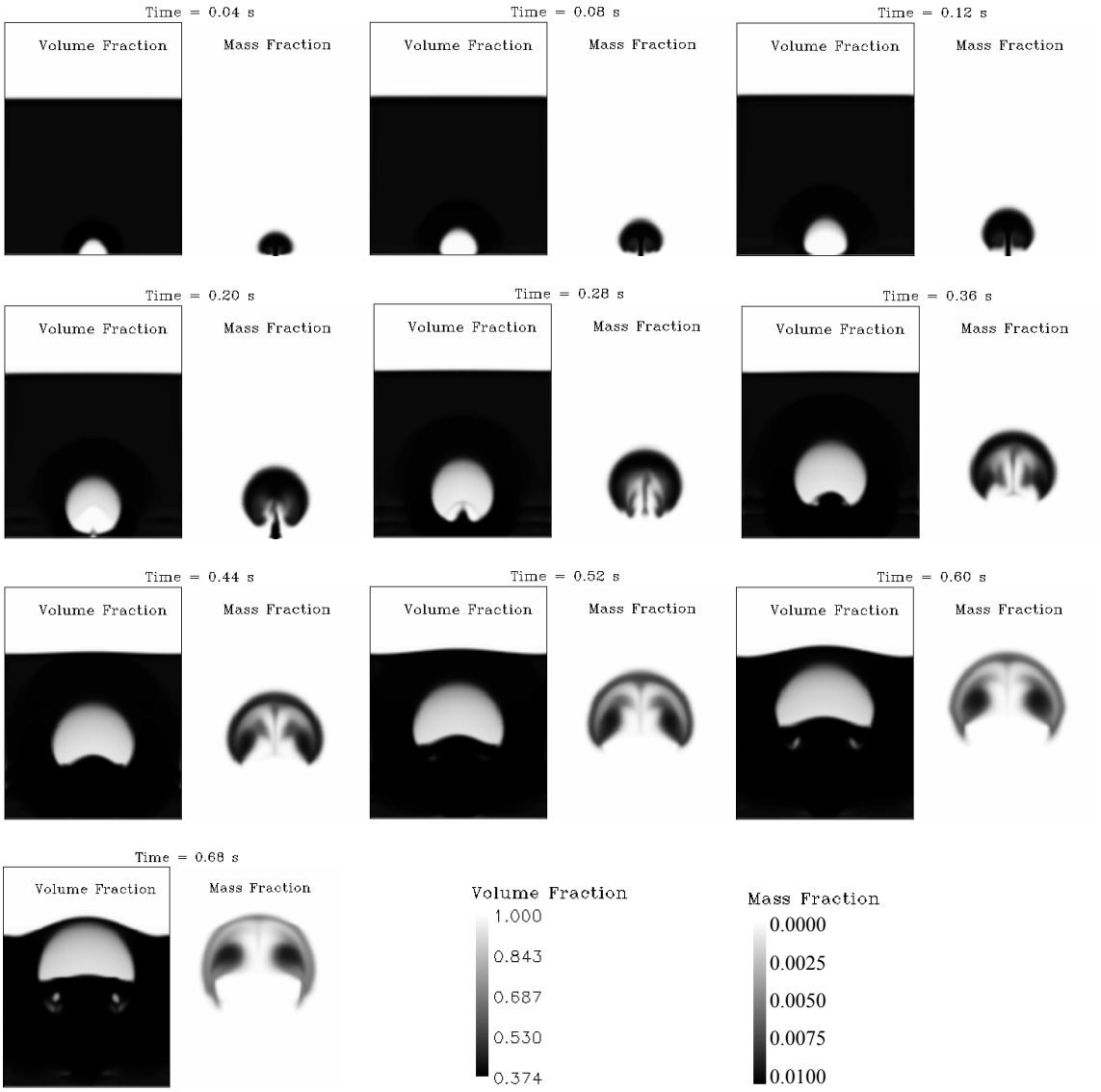

Figure 2: Snapshots of the volume fraction of the gas phase and the mass fraction of tracer gas in the fluidized bed at different times after starting the jet. (dp=460 μm, jet velocity= 7 m/s, opened for 0.2 s).

Uniform concentration of tracer in the bubble?

In order to clarify the mechanism of mass transfer, the streamlines and a vector plot of the gas phase velocity including the bubble contour is shown in Figure 3. Additionally, a surface plot of the mass fraction of the tracer gas with respect to bubble contour is given to indicate the extent of mass transport of tracer gas from the bubble. Figure 3 clearly shows that fluidizing gas is continuously introduced into the bubble at the lower boundary of the bubble, while simultaneously gas leaves the bubble at the upper boundary carrying tracer gas with it. The tracer gas was transported out of bubble in the direction of the gas flow indicating that in a fluidized bed filled with 460 μm particles the transfer of the tracer gas is mainly controlled by convection (through- flow) rather than diffusion. Furthermore, at both sides of the bubble in the lateral direction, two vortices emerge creating a circulation pattern of the gas. The surface plot of the mass fraction of the tracer gas also reveals that the concentration of tracer in the bubble is not uniform and that it is dilute in the lower and central part of the bubble. Due to recirculation of the tracer back into the bubble the tracer concentration was much higher at both sides of the bubble.

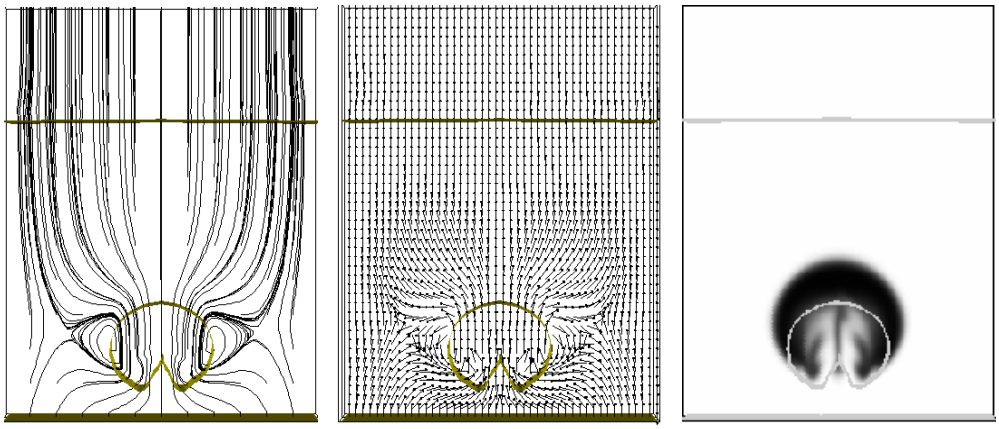

(a) (b) (c)

Figure 3: (a) Gas velocity streamlines, (b) gas velocity vector plot and (c) mass fraction distribution of the tracer gas with respect to the bubble contour at 0.28 s in single bubble simulations (d_p=460 μm, average bubble diameter=0.165 m). Other conditions are listed in Table 1.

Constant bubble diameter?

To calculate the bubble-to-emulsion phase mass transfer coefficient the diameter of the bubble and the average concentration of the tracer in the bubble was calculated (see Figure 4). During the first 0.2 s the bubble was formed at the nozzle. However, the bubble also grows when it rises through the bed after the bubble detached from the nozzle. The bubble growth under these conditions was also reported by other researchers (e.g. Sit and Grace, 1973). Due to the path of least resistance, gas flows through the bubble and the equivalent diameter of the bubble increases, which involves deaeration of the emulsion phase. The average concentration of the tracer gas in the bubble strongly decreases during the formation of the bubble. The rate of decrease in the concentration of tracer gas was constant till 0.3 s and decreased after that.

When developing empirical correlations for the bubble-to-emulsion phase mass transfer coefficient usually the change in the concentration of tracer gas (mostly ozone) in a single isolated rising bubble in a pseudo two-dimensional or three-dimensional fluidized bed was measured using a UV absorption technique (Chiba and Kobayashi, 1970; Chavarie and Grace, 1976; Sit and Grace, 1978). These researchers measured the concentration of tracer gas in the bubble at different heights above the injection point. As described by Chavarie and Grace (1976) and Sit and Grace (1978) the experimental set-up consisted of a UV source and a photo multiplier placed at different heights in the center of the bed. Therefore, it is likely that the concentration of the tracer gas measured was the central concentration of the tracer gas. However, since our simulations clearly reveal that the concentration of tracer gas is not uniform in the bubble, the central concentration does not represent the average concentration of the tracer gas in the bubble. The simulation showed that the concentration of the tracer in the centerline of the bubble was indeed decreasing while the bubble rises through the bed, while the average concentration hardly changes.

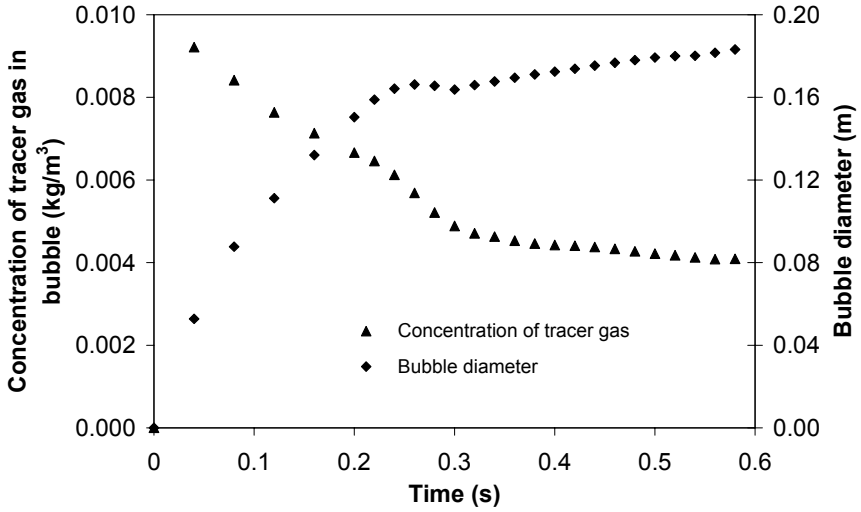

Figure 4: Concentration of the tracer gas in the bubble and the equivalent diameter of the bubble as function of time for a single injected bubble (d_p=460 μm, jet velocity = 7 m/s, other conditions are listed in Table 1).

Constant mass transfer coefficient?

Since the size of the bubble is growing during its path through the bed, the determination of the mass transfer rate from the decrease in the average concentration of the bubble is illusive. In order to take the net transport of the tracer gas from the bubble to the emulsion phase into account, the total quantity of tracer gas in the bubble as a function of time is presented in Figure 5. During the formation of the bubble (< 0.2 s) the total amount of the tracer gas in the bubble is increasing. Immediately after the detachment of bubble from the nozzle, the tracer quantity in the bubble decreased significantly (0.2 – 0.3 s) but remains constant afterwards. As depicted in Figure 3, the circulation of the gas at the sides of the bubble, reintroduces the tracer gas back into the bubble. A balance between tracer gas leaving at the upper boundary and tracer gas reintroduced at the sides of the bubble results in an almost constant tracer amount in the bubble.

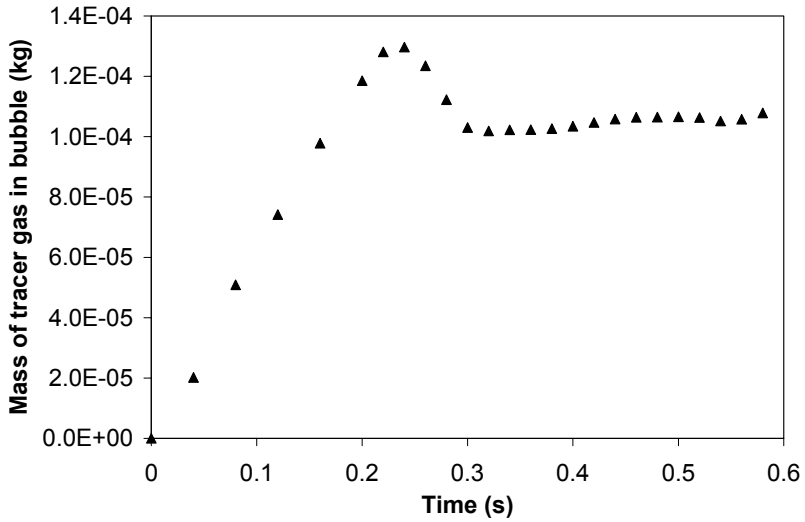

Figure 5: Total mass of the tracer gas in the bubble and the diameter of the bubble versus time for single bubble simulations (d_p=460 μm, jet velocity= 7 m/s).

In industrially operated fluidized bed reactors, especially when fast chemical reactions, the recirculation of chemical species is much less pronounced, since the reactants leaving the bubble interface are converted in the

emulsion phase before they can be reintroduced into the bubble. Therefore, the transport of mass from the bubble to the emulsion phase was studied using the model where it was assumed that the tracer was reacting with an infinitely fast reaction rate in the emulsion phase. This can be expressed as,

$$\frac{\partial(\varepsilon_f \rho_f \omega_{Af})}{\partial t} + \nabla \cdot \left(\varepsilon_f \left(\rho_f \bar{\boldsymbol{u}} \omega_{Af} - D_{eff,A} \nabla \omega_{Af} \right) \right) = \varepsilon_f k_{Af} \rho_f \omega_{Af} \tag{18}$$

where k_{Af} is the reaction rate constant for which a very high value was taken (10^6 s^{-1}). Figure 6 shows the fraction of the initial tracer quantity remaining in the bubble while rising in the bed for the test case with and without tracer reactions in the emulsion phase. For the case with an infinitely fast reaction of tracer gas in the emulsion phase, the tracer quantity in the bubble is continuously decreasing due to transfer of tracer to the emulsion phase without recirculation of tracer gas back into the bubble. The graph shows that the predicted rate of decrease in tracer quantity in the bubble (slope) decreases after 0.1 s after detachment of bubble. The flow across the bubble boundary changes along the bubble contour and it is higher in the center and decreases along the side of the bubble (see also Kuipers, 1990). Therefore, the tracer gas from the center of the bubble is transported to the emulsion phase with a higher rate, until the center of the bubble is depleted of tracer gas. Subsequently, only tracer gas from the side of the bubble is exchanged at a lower rate. Szekely (1962) and Chiba and Kobayashi (1970) also concluded from their experiments that a larger part of the transfer took place immediately after bubble formation.

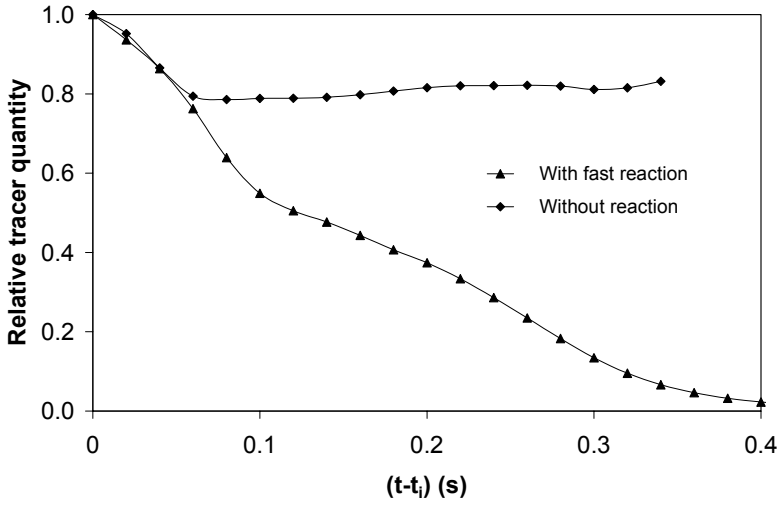

Figure 6: Comparison of the fraction of the initial tracer amount remaining in the bubble while rising in the bed for the case where the tracer is infinitely fast converted into phase and the case without reaction.

Concluding, the model results have shown that the usual assumption used in the phenomenological models, mainly that the bubble diameter remains constant, that the tracer concentration is uniform in the bubble, and that the mass transfer coefficient remains constant are not valid. Therefore, the assumption of a constant mass transfer coefficient is also not valid.

5.2.2 Bubble to emulsion phase mass transfer coefficient

Consider a single clouded bubble, containing tracer A with an initial concentration C_{Ai} (mass of tracer A per unit volume) injected at time t_i into a fluidized bed with an emulsion phase concentration of C_{Ae}. The rate of change in the average tracer concentration in the bubble (C_{Ab}) is expressed as,

$$-u_b \frac{dC_{Ab}}{dz} = K_{be} \left(C_{Ab} - C_{Ae} \right) \tag{19}$$

where, u_b represents the bubble rise velocity and z the vertical distance traveled by the bubble. The amount of the tracer in the emulsion phase remains negligibly small, if the volume of the tracer gas injected is much less than the bed volume. Integration of equation (19) yields,

$$\frac{C_{Ab}}{C_{Ai}} = \exp\left[-\frac{K_{be}(z-z_i)}{u_b}\right] \tag{20}$$

where K_{be} (s^{-1}) is the mass exchange coefficient. The mass transfer coefficient is defined per volume bubble phase and therefore, the overall mass transfer coefficient k_m (m/s) can be calculated from the two-dimensional simulations using:

$$k_m = \frac{Area}{Circumference} K_{be} = \frac{d_b}{4} K_{be} \tag{21}$$

Thus equation (20) becomes,

$$\frac{C_{Ab}}{C_{Ai}} = \exp\left[-\frac{4k_m(z-z_i)}{D_b u_b}\right] \tag{22}$$

or alternatively

$$\frac{C_{Ab}}{C_{Ai}} = \exp\left[-\frac{4k_m(t-t_i)}{D_b}\right] \tag{23}$$

Equation (23) is valid only if the bubble diameter and mass transfer coefficient remain constant while the bubble rises through the bed. Since the bubble is growing, a time period was chosen (0.24 s –0.32 s) for which the variation in the bubble diameter was within 5% of the average bubble diameter (0.165 m) and recirculation of tracer gas into the bubble was still absent when calculating a mass transfer coefficient from the simulations results. Taking the initial concentration of the bubble equal to the average concentration at 0.24 s, the initial bubble-to-emulsion phase mass transfer coefficient was calculated from slope of the graph where $\ln\left(\frac{C_{Ab}}{C_{Ai}}\right)$ was plotted as a function of $(t-t_i)$, which yielded 0.137 m/s. Table 5 compares the calculated bubble-to-emulsion phase mass transfer coefficient with predictions from different phenomenological models listed in Table 4. The model from Davidson and Harrison (1963), which accounts for both convective and diffusive contributions, estimates the mass transfer coefficient close to the simulation results for different particle diameters and bubble sizes. On the other hand the model from Chiba and Kobayashi (1970), which only accounts for diffusive transport underestimates the mass transfer coefficients with an order of magnitude compared to the simulation predictions. This indicates that for a wide range of particle diameters the convective transport is more important than the diffusive transport.

Table 5: Comparison of the simulated bubble-to-emulsion phase mass transfer coefficient with predictions from phenomenological models taken from the literature.

Particle size (μm)	Average Bubble diameter (m)	Mass Transfer coefficient (m/s)		
		Simulation	Chiba and Kobayashi (1970)	Davidson and Harisson (1963)
460	0.165	0.137	2.90×10^{-3}	0.128
460	0.095	0.158	2.49×10^{-3}	0.129
100	0.157	0.021	5.13×10^{-3}	0.018

5.2.3 Effect of the bubble diameter on the bubble-to-emulsion mass transfer

The effect of the bubble diameter on the bubble-to-emulsion phase mass transfer coefficient was studied for a fluidized bed containing 460 μm particles by comparing the relative amount of tracer remaining in the bubble while it rises through the bed for two different bubble sizes with an average diameter of 0.165 m and 0.095 m (see Figure 7). The larger bubble was introduced in the minimum fluidized bed by opening jet with velocity 7 m/s for 0.2 s, while the smaller bubble was generated by opening the jet with 3.5 m/s for 0.16 s. Figure 7 shows that for both bubble sizes the tracer quantity in the bubble strongly decreases initially and later remains almost constant for the larger bubble and increases slightly for the smaller bubble due to recirculation of the tracer gas back into the bubble.

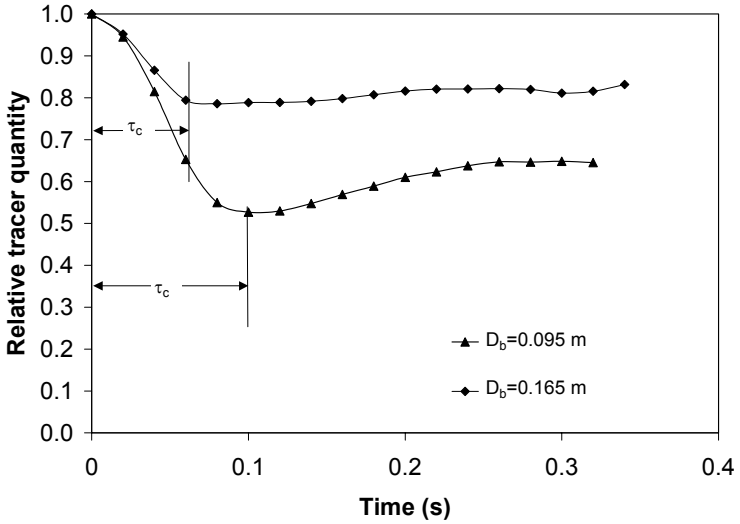

Figure 7: Fraction of the initial tracer quantity present in the bubble as a function of time for bubbles with different average diameter.

The reintroduction of the tracer gas into the bubble starts some time after the detachment of the bubble from the nozzle. This time is characterized with a circulation time constant (τ_c), which is the time required for the tracer gas to be recirculated back into the bubble after having left from the upper boundary. The circulation time will be smaller in case of high 'throughflow' of gas through the bubble and therefore inversely proportional to the relative bubble velocity. The circulation time is indeed smaller for larger bubble (see Figure 7). In Table 5 the calculated bubble-to-emulsion phase mass transfer coefficient for both bubble sizes is compared with the predictions from the phenomenological models. The simulations showed that the mass transfer coefficient increased with about 15% for the smaller bubble. The additive diffusion-convection model by Davidson and Harrison (1963) strongly underestimates the effect of the bubble diameter, while the diffusion controlled model by Chiba and Kobayashi (1970) under-predicts the mass transfer coefficients with more than an order of magnitude and even predicts the opposite effect of the bubble size.

5.2.4 Effect of the particle diameter on the bubble-to-emulsion mass transfer

The exchange of mass from the bubble to the emulsion phase is strongly influenced by the particle size. Figure 8 illustrates the simulated gas velocity and mass fraction distribution of the tracer gas with respect to the bubble contour for a single bubble rising through a bed filled with 100 μm particles. It shows that the tracer gas is almost completely contained inside the bubble, unlike the bubble rising in a bed filled with 460 μm particles, where tracer was leaving the bubble boundary due to gas flowing through the bubble. Figure 8 shows that for the 100 μm particle case recirculation of tracer gas is absent.The bubble-to-emulsion phase mass transfer coefficient predicted for different particle sizes and approximately the same bubble size was also listed in Table 5. The mass transfer coefficient strongly decreases for smaller particles. The diffusion-controlled model (Chiba and Kobayashi, 1970) predicted again very low values for the mass transfer coefficient but additionally shows an increase in mass transfer coefficient with a decrease in particle size. The additive diffusion-convection model (Davidson and Harrison, 1963)

estimates values for the mass transfer coefficient close to the simulation results. For small particles the drag force experienced by the particles is high resulting in small flow through the bubble compared to the case with large particles. Thus the convective contribution to the bubble-to-emulsion phase mass transfer is decreased for small particles leading to lower mass transfer coefficients.

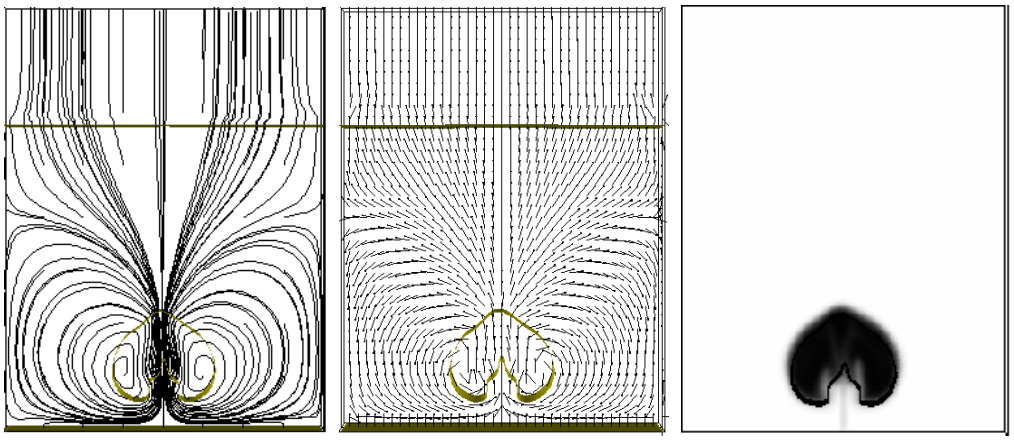

(a) (b) (c)

Figure 8: Gas velocity (a) streamlines, (b) vectors and (b) mass fraction of tracer gas with respect to bubble contour at 0.28 s after the start of the jet in the bed filled with particle size of 100 μm (jet velocity = 7 m/s, opened for 0.2 s, average bubble diameter=0.157 m).

5.2.5 Influence of the effective diffusivity

Although for all the simulations reported in this paper the effective diffusivity of the gas phase was expressed by equation (16) which accounted for the tortuous path of the gas phase as well as micro scale convective flow, calculations were also carried out where only the molecular diffusivity of the gas phase taken into account. The calculations showed that the mass transfer coefficient is not influenced by the gas phase diffusivity proving that the convective contribution is completely dominating the diffusional contribution for the case under consideration. For larger particles the effect of the tortuous path as well as the micro scale convection patterns will have more influence resulting in higher gas phase diffusivites.

6. BUBBLING FLUIDIZED BED WITH A JET

In the previous section, the bubble-to-emulsion phase mass transfer was studied for a single bubble rising through a bed at incipient fluidization conditions to obtain more insight in the mechanism of mass transfer. However, in a bubbling fluidized bed, the gas dispersion is much more complex. Bubbles are generated at the gas distributor and while rising through the bed they coalesce and break up. Although the two-phase phenomenological models take into account bubble growth for a bubbling fluidized bed, they do not consider the variation of concentration in the radial direction, which could be important if reactants are not premixed before being introduced into the fluidized bed. In this part of the study, experiments were carried out to study the radial dispersion of the tracer gas in a pseudo two-dimensional bubbling fluidized bed (0.3 m×1.0 m×0.015 m) with a jet in the center. Initially the bed was operated at incipient fluidization conditions with a bed height of 0.4 m and subsequently gas with a velocity higher than the minimum fluidization velocity was injected through the orifice in the center of the bed. The measured concentration profiles in the bed were compared with numerical simulations.

6.1 Results and discussion

With the continuous introduction of gas through the jet continuously bubbles were generated at the nozzle, which propagated through the bed. A tracer gas, which was introduced in the bed via the jet, was dispersed in the bed. Figure 9 shows snap shots of the gas phase volume fraction and the tracer gas mass fraction distribution at different time intervals in the fluidized bed filled with 460 μm particles, using a continuous jet with a gas velocity of 0.95 m/s. The bubbles formed at the nozzle were rich in tracer gas and while rising through the bed these bubbles

exchange gas with the emulsion and they also coalesce with leading bubbles. Furthermore, the bubble size increases and their shape changes to cap-shaped, which enhances convective flow in the radial direction. The tracer concentration in the freeboard region was approximately uniform. The simulation results showed unrealistic symmetry of the flow patterns in the initial time period due to idealistic boundary conditions, which however vanished after about 2.0 s. A snap shot at 6.0 s showed flow through jet deviating from the center resulting in bubbles to rise off center, promoting radial dispersion in the bed.

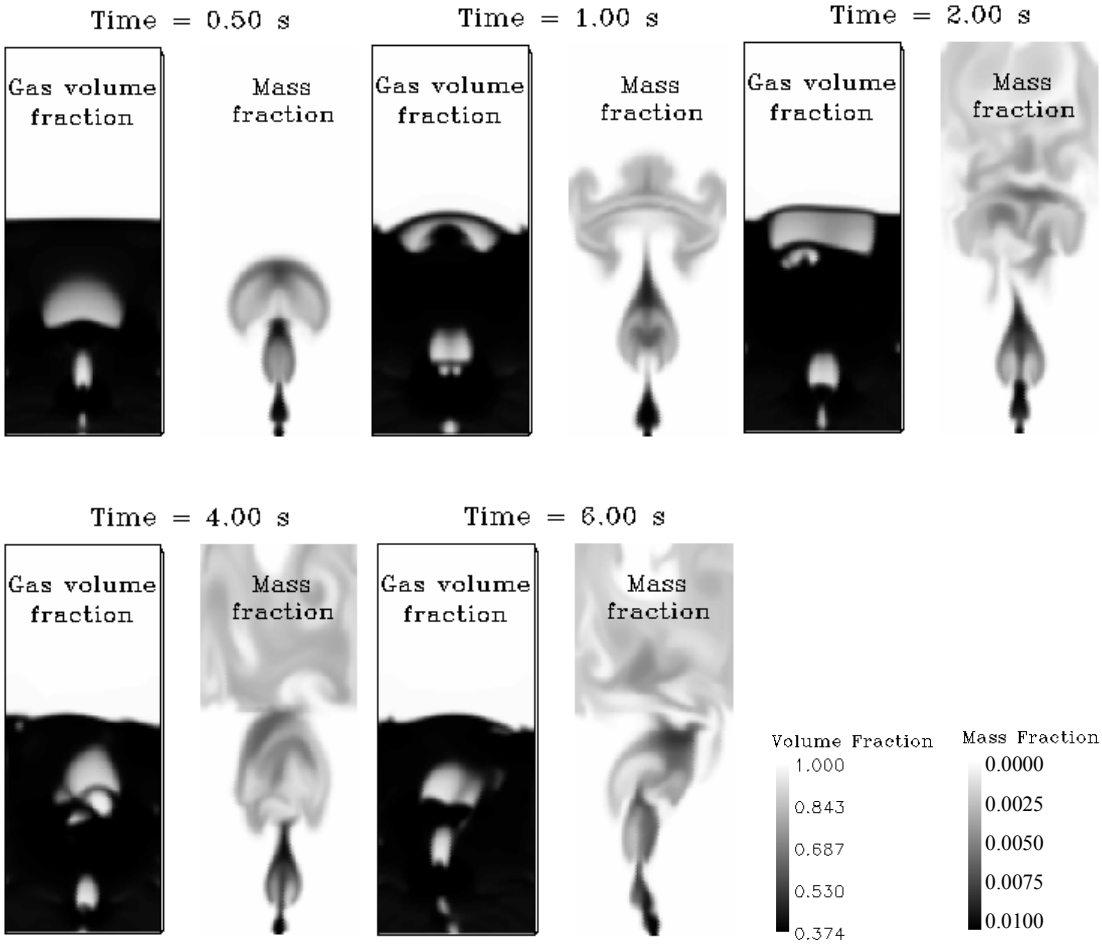

Figure 9: Snap shots of the gas phase volume fraction and tracer gas mass fraction distribution in the fluidized bed filled with 460 μm particles, at different time intervals after the introduction of bubbles with a jet with a velocity of 0.95 m/s.

Since the percolation of tracer gas into the fluidized bed is very dynamic, time-averaged concentrations were determined by averaging over a period of 8 s (averaging of longer period did not influence the results). In Figure 10(a) a surface plot of the time-averaged mass fraction of the tracer gas in the bed is given showing the increase in the distribution of tracer gas at higher axial positions in the bed. The radial variation of the relative time averaged concentration of the tracer gas at different heights in the bed filled with 460 μm particles for jet velocity of 0.95 m/s predicted by the model are compared with the experimental results in Figure 10(b). In the center, the concentration of the tracer gas is higher which decreases with increase in height above the distributor. However, away from center the time-averaged concentration of tracer gas increases with increase in height above the distributor. While rising through the bed, the size of the bubble, which are rich in tracer gas, increases and its shape changes to cap-shaped both promoting convective flow in radial direction resulting in increase in radial dispersion. The predicted time-averaged concentration of tracer gas at 0.3 m above the distributor showed very good agreement

with the experimental results. Although, at 0.1 m above the distributor, the concentration of tracer gas was slightly over-predicted in the center, it showed good agreement with experimental data further away from the center.

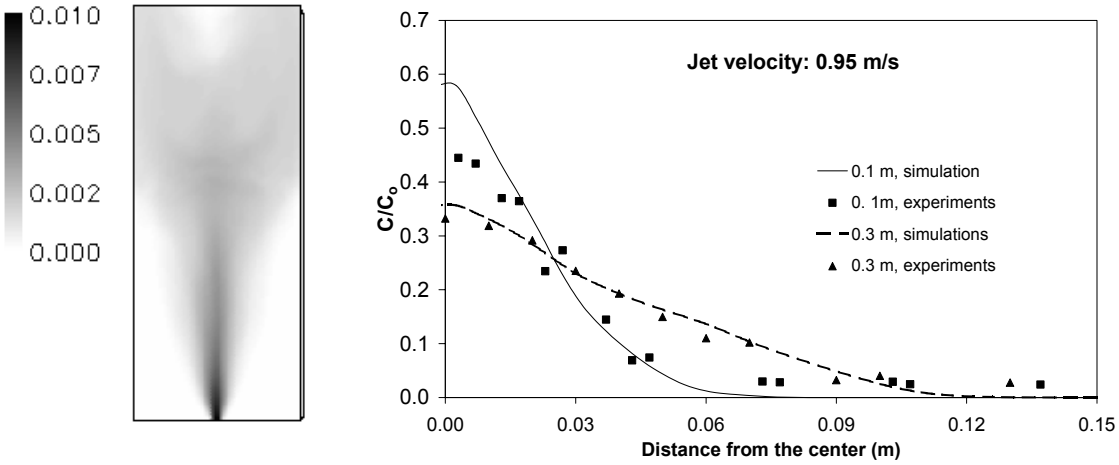

(a) (b)

Figure 10: (a) Surface plot of time averaged mass fraction of tracer gas in the bed after 8 s. (b) Experimental comparison of the relative time-averaged radial concentration profiles of the tracer gas at different heights in the fluidized bed (d_p=460 μm and jet velocity=0.95m/s).

6.1.1 Influence of the jet velocity on the radial dispersion

The jet velocity has a significant influence on the radial dispersion, which was studied by comparing the predicted time-averaged concentration of tracer gas for a jet velocity of 0.95 m/s and 3.8 m/s at 0.1 m above the distributor in the fluidized bed containing particles of 460 μm with experimental measurements (see Figure 11). Away from the center the concentration of tracer gas increases with an increase in the jet velocity, which indicates that the radial dispersion in the bed increases with higher jet velocity. For higher gas velocities through the jet, larger bubbles are formed at the nozzle, which increases the throughflow of bubbles resulting in increased convection in the radial direction.

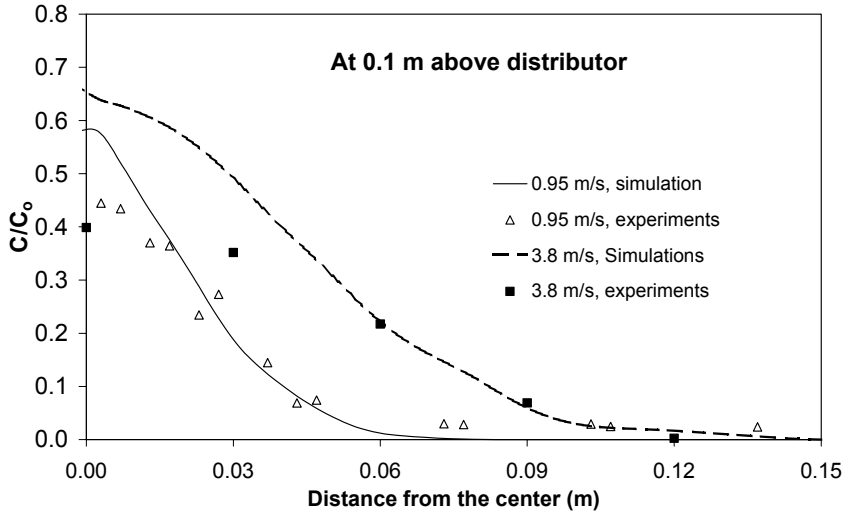

Figure 11: Experimental comparison of the predicted time-averaged radial profiles of the tracer gas concentration inside the fluidized bed 0.1 m above the distributor for different jet velocities (d_p=460μm).

The simulated time-averaged concentration of tracer gas showed good agreement with the experimental measurement in predicting the increase in the radial dispersion with an increase in the jet velocity. However, the time-averaged concentrations of tracer gas at a jet velocity of 3.8 m/s were over-predicted in the center of the bed compared to the experimental data. In the experiments the jet showed significant "meandering" behavior at higher jet velocities, which could be responsible for the higher radial dispersion of tracer gas resulting in lower concentrations in the center of the fluidized bed. Due to the idealistic boundary condition of steady and uniform inlet velocity through the jet and the porous plate, smaller meandering behavior of the jet was predicted in the simulations, which could be a plausible explanation for this discrepancy. Note that width of the tracer distribution is in the order of the average bubble diameter.

6.1.2 Influence of the particle diameter

The particle diameter is one of the most important parameters influencing the gas dispersion in a fluidized bed. Figure 12 gives a comparison of the time-averaged concentration of the tracer gas measured and predicted by the model for 460 μm and 700 μm particles at 0.1 m above the distributor with a jet velocity of 3.8 m/s. The time-averaged concentration of the tracer gas in the center of the bed increased with an increase in the particle diameter. However, away from center it decreases with increase in particle size. Indeed, for larger particles the drag experienced by the solid phase is less resulting in a higher convectional flow through the bubble and therefore more axial dispersion and less radial dispersion of tracer gas was observed compared to smaller particles. The predicted time-averaged concentration of tracer gas showed good qualitative agreement with the experiments showing the strong decrease in the radial dispersion for the large particles. However, for the fluidized bed filled with 700 μm particles the concentration of the tracer gas was over-predicted compared to experimental measurements.

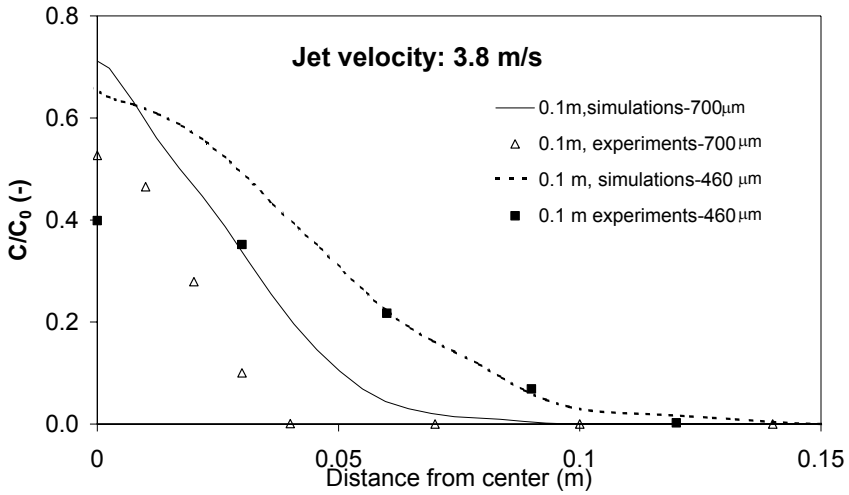

Figure 12: Comparison of the time-averaged concentration profile predicted inside the fluidized bed at 0.1 m above the distributor for 460 μm and 700 μm particles for the jet velocity of 3.8 m/s.

7. CONCLUSIONS

The simulation of a single rising bubble through an incipiently fluidized bed containing 460 μm particles shows that fluidizing gas is continuously introduced into the bubble at the lower boundary of the bubble indicating that the transfer of the tracer gas is mainly controlled by convection (throughflow) rather than diffusion. The simulation results showed that the usual assumptions often used in phenomenological models for the prediction of the bubble-to-emulsion phase mass transfer coefficient, mainly that the bubble diameter remains constant and that the tracer concentration is uniform in the bubble are not valid. Due to the non-uniform flux of fluidizing gas across the bubble boundary and non-uniform concentration of tracer gas inside the bubble, the assumption of a constant mass transfer coefficient also does not hold. For large particles, the gas leaving the upper bubble boundary is recirculated thereby reintroducing the tracer back into the bubble, which eventually results in an almost constant tracer amount in the bubble. Simulations results have shown an increase in the initial bubble-to-emulsion phase mass transfer coefficient

for large bubbles and for large particles. This could be attributed to an increase in the throughflow through the bubble and the corresponding increase in the convective contribution to the bubble-to-emulsion phase mass transfer. The comparison of the simulated mass transfer coefficient with predicted values from phenomenological models showed good agreement with a literature correlation assuming additive convection-diffusion transport (Devidson and Harrison, 1963). The model that only accounts for diffusive transport (Chiba and Kobayashi, 1970) strongly underestimated the mass transfer coefficient for different bubble sizes and different particle sizes.

In a bubbling fluidized bed, continuously bubbles containing tracer gas were generated at the nozzle, which propagated through the bed. While rising through the bed, the size of the bubble, which are rich in tracer gas, increases and their shape changes to cap-shaped, which enhances convective flows in the radial direction. The simulated results showed very good agreement with the experimental measurements especially for lower jet velocities. With an increase in the jet velocity the radial dispersion increases due to an increase in size and frequency of the bubbles and thus an increase in the radial convection. However, in the center, the concentration of tracer gas is somewhat over-predicted, possibly due to under-prediction of the meandering of jet. The decrease in the radial dispersion for large particles predicted by the model agreed well with the experimental data.

8. ACKNOWLEDGEMENT

This work is a part of the research program of the Dutch Research School on Process Technology, 'OnderzoekSchool Proces Technologie (OSPT)'. It is financially supported by Akzo Nobel, DSM and Shell Research.

9. NOTATIONS

$\boldsymbol{C}$	Fluctuating velocity of the particulate phase
$C_{A,b}$	Concentration of tracer gas in bubble
$C_{A,i}$	Concentration of tracer gas in the bubble at initial time
C_d	Drag coefficient
C_o	Concentration of tracer gas at the inlet of fluidized bed
D_b	Bubble diameter
D_c	Cloud diameter
D_{eff}	Effective diffusivity of tracer gas in fluidized bed
D_f	Molecular diffusivity of tracer gas
D_{ij}	Strain rate
d_p	Particle diameter
e	Restitution coefficient for particle-particle collision
F, r and s	Empirical constants of equation (14)
g	Gravitational acceleration
g_o	Radial distribution function
k_m	Bubble to emulsion phase mass exchange coefficient
m	Particle mass
$\overline{u}$	Mean gas phase velocity
$\overline{v}$	Mean solid phase velocity
p	Pressure
P_c	Critical state pressure
$\boldsymbol{q}_s$	Kinetic fluctuation energy flux
Re_p	Particle Reynolds number
t	Time
u_b	Bubble rise velocity
u_{mf}	Superficial gas velocity at minimum fluidization condition
z	Height above distributor

Greek letters

α	Ratio of rising velocity of bubble to that of the interstitial gas in emulsion phase
β	Interphase momentum transfer coefficient
γ	Dissipation rate due to inelastic particle-particle collisions
ε	Volume fraction
ε_{min}	Minimum solid volume fraction above which frictional stresses are effective (ε_{min}=0.5)
$\varepsilon_s^{\max}$	Solid volume fraction at packed condition ($\varepsilon_s^{\max}$ =0.64536)
Θ	Granular temperature
κ	Conductivity of the granular fluctuating energy.
λ	Bulk viscosity
μ	Shear viscosity
ρ	Density
τ	Shear stress tensor
ϕ	Angle of internal friction
ω	Mass fraction of the tracer gas

Subscripts

f	Gas phase
s	Solid phase
w	Wall

Superscripts

f	Frictional
kc	Kinetic and collisional

10. REFERENCES

Atkinson, J.H. and Bransby, P.L., The Mechanics of Soils: An Introduction to Critical State Soil Mechanics. , McGraw-Hill, England, (1978).

Chapman, S. and Cowling, T.G., "The mathematical theory of non-uniform gases", 3rd edition, Cambridge university press, Cambridge, (1970).

Chavarie, C. and Grace, J.R., "Interphase mass transfer in a gas-solid fluidized bed", Chem. Eng. Sci., Vol. 31, 741-749, (1976).

Chiba,T. and Kobayashi, K., "Gas exchange between bubble and emulsion phases in gas-solid fluidized beds", Chem. Eng. Sci., Vol. 25, 1375-1385, (1970).

Davidson, J.F. and Harrison, D., "Fluidized particle", Cambridge University Press, (1963).

Ding, J. and Gidaspow, D., "A bubbling fluidization model using kinetic theory of granular flow", AIChE J., Vol. 36, 523-538, (1990).

Ergun, S. "Fluid flow through packed columns", Chem. Eng Prog., Vol. 48, 89-94. (1952).

Gidaspow, D., "Multiphase flow and fluidization: Continuum and kinetic theory descriptions", Academic press, Boston, (1994).

Guenther, C., O'Brien, T. and M. Syamlal, "A Numerical Model of Silane Pyrolysis in a Gas-solids Fluidized Bed," Proceedings of the International Conference on Multiphase Flow 2001 in New Orlears Louisiana May 27-June 1 (2001)

Gunn, D.J., "Axial and radial dispersion in fixed bed, Chem". Eng. Sci., Vol. 42, 363-373, (1987).

Jackson, R. In: R. Meyer, Editor, "Theory of Dispersed Multiphase Flow", Academic Press, New York, p. 291, (1982).

Jenkins, J.T. and Savage, S.B., "A theory for the rapid flow of identical, smooth, nearly elastic, spherical particles", J. Fluid Mech., Vol. 130, 187-202, (1983).

Johnson, P.C. and Jackson, R., "Frictional-collisional constitutive relations for granular materials, with application to plane shearing", J. Fluid Mech., Vol. 67, 176, (1987).

Koch, D.L. and Hill, R.J., "Inertial effects in suspension and porous-media flows", Annu. Rev. Fluid Mech., Vol. 33, 619-647, (2001).

Kuipers J.A.M., "A two-fluid micro balance model of fluidized bed", Ph.D. Thesis, Twente University, Enschede, The Netherlands, (1990).

Ma, D. and Ahmadi G., "An equation of state for dense rigid sphere gases", J. Chem. Phys., Vol. 84, No. 6, 3449-3450, (1986)

Nieuwland, J.J., "Hydrodynamic modeling of gas-solid two-phase flows", Ph.D. Thesis, Twente University, Enschede, The Netherlands, (1995).

Punčochář, M. and Drahoš J., "The tortuousity concept in fixed and fluidized bed", Chem. Eng. Sci. Vol. 48, 2173-2175, (1993).

Samuelbsberg, A. E., "Modelling and simulation of fluidized bed reactors", Ph.D. Thesis, Norwegian institute of technology, university of Trondheim (1994)

Savage, S.B., "Analyses of slow high-concentration flows of granular materials", J. Fluid Mech., Vol. 377, 1, (1998).

Savage, S.B., Proc. US– Japan Seminar on "New Models and Constitutive Relations in the Mechanics of Granular Materials", in: J.T. Jenike, M. Satake (Eds.), Elsevier, p. 261, (1983).

Sinclair, J.L. and Jackson, R., "Gas-particle flow in a vertical pipe with particle-particle interactions", AIChE J., Vol. 35, 1473, (1989).

Sit, S.P. and Grace, J.R., "Interphase mass transfer in an aggregative fluidized bed', Chem. Eng. Sci., Vol. 33, 1115-1122, (1978).

Srivastava, A. and Sundaresan, S., Analysis of a frictional–kinetic model for gas–particle flow, Powder Technology, Vol. 129, 72-85, (2003).

Szekely J., "The interaction between fluids and particles", Instn. Chem. Engrs, London, 197, (1962).

Wen, Y.C. and Yu, Y.H., "Mechanics of fluidization", Chem. Eng. Prog. Symp. Ser., Vol. 62, 100-111, (1966).

Werther, J., Chem. Ing. Tech., Vol. 49, No. 11, p. 777, (1977).